SUPPORTING INFORMATION

for

Electrostatics of nucleic acid folding under conformational constraint

Peter C. Anthony, Adelene Y.L. Sim, Vincent B. Chu,
Sebastian Doniach, Steven M. Block, and Daniel Herschlag

Contents:

1. SUPPORTING EXPERIMENTAL PROCEDURES

Dumbbell preparation

The 20R55/4T DNA hairpin[1], having a 20-bp stem and a thymidine tetraloop, was obtained as part of a PAGE-purified, chemically synthesized oligonucleotide (IDT), sequence `5′-atcgagagggacacggggaaacacc_GAGTCAACGTCTGGATCCTGTTTTCAG GATCCAGACGTTGACTC_catcatcctgactagagtccttggc-3′`, in which each end of the hairpin sequence (uppercase) was flanked by an abasic site ("_") and 25 additional nucleotides (lowercase). Double-stranded DNA handles were then prepared with single-stranded overhangs complementary to the flanking sequences in order to link the hairpin to beads. A 2,018-bp handle with a 5′ overhang and a digoxygenin label at the opposite end was prepared by PCR, using one autosticky primer[2], one 5′-digoxygenin-modified primer, and the M13mp18 plasmid as the template. A 1,044-bp handle with a 3′ overhang and a biotin label at the opposite end was prepared by PCR templated on the pALB3 plasmid, using one primer containing a phosphorothiote bond and one 5′-biotin-modified primer, followed by digestion with lambda-exonuclease[3]. All primers were obtained from IDT, and both handles were gel-purified and ethanol-precipitated. The hairpin was annealed to the handles in STE+ buffer (100 mM NaCl, 10 mM Tris-HCl, 10 mM EDTA, pH 8.0), with all components at ~20 nM, by lowering the temperature from 80 to 25 °C over 30 minutes. The annealing reaction was then diluted 300- or 900-fold in phosphate buffer (100 mM sodium phosphate, 3 mg/mL BSA, pH 7.5) and incubated with 0.6 μm-diameter avidin-coated beads and 0.73 μm-diameter anti-digoxigenin-coated beads (each ~50 pM in phosphate buffer) at room temperature for 1 hour to form dumbbells.

Buffers

Solutions at 40, 100, 200, 500 and 1000 mM of each of five monovalent cations (Li^+, Na^+, K^+, Rb^+, and TMA^+) were used for hairpin measurements, as well as solutions containing 40 or 200 mM K^+ and 1, 2, 5, or 10 mM $MgCl_2$. All ionic solutions were buffered with 50 mM MOPS. The first 40 mM of each monovalent cation was added as the hydroxide salt in order to raise the pH to 7.5; the rest was added as the chloride salt. Dumbbells were diluted 1:30 into the working buffer, consisting of the buffered salt solution and 2% (v/v) oxygen scavenger (250 mg/mL glucose, 37 mg/mL glucose oxidase, 1.7 mg/mL catalase), and flowed onto a microscope coverglass. All ionic concentrations stated in this work are for the starting buffered solutions, excluding the 5% dilution and introduction of trace ions (most significantly, 3.3 mM sodium phosphate) resulting from the addition of dumbbells and oxygen scavenger. However, all calculations (*mfold*, Poisson-Boltzmann and HEL) took these effects into account, so that calculation results and experimental data are directly comparable.

Numerical data and error analysis

All experimental values of Δx and $F_{1/2}$ (see **Figures 3 and 4** and **Tables S4-S8**) are reported as the mean ± total uncertainty, which includes the statistical standard error of the mean (calculated by bootstrap analysis) added in quadrature to estimates of systematic uncertainties in the optical trapping assay. The systematic uncertainty in Δx was estimated to be 2%, corresponding to a ~10-15 nm uncertainty in our measurement of the position of the zero-stiffness region (ZSR) of the weak trap. The systematic uncertainty in $F_{1/2}$ included 5% to account for variation in the trap stiffness measurements made on the same day and changes to these measurements observed over time, as well as the uncertainties in stiffness due to the refractive index of the buffer (~1%) and

the temperature (<1%). As ΔG is the product of Δx and $F_{1/2}$, all of the uncertainties in Δx and $F_{1/2}$ are propagated into the uncertainty of ΔG.

Generating ensembles of models for Poisson-Boltzmann calculations

The initial structural models (folded and unfolded) were energy-minimized (Amber 94 potential[4], allowing only atoms linking the hairpin to the DNA handles to move) to reduce excess bond-length strains, and then randomized using implicit solvent molecular dynamics simulations as implemented in NAB[5]. A time step of 1 fs was used in all simulations, with snapshots taken after every simulated annealing routine (from 500 K to 300 K in steps of 100 K, with 100,000 steps at each temperature). Electrostatics were accounted for by assuming a solvent dielectric constant of 80 (see **Table S2** for a discussion of other methods). For the folded model, only the residues in the loop and those adjacent to the handle fragments were allowed to move, while for the unfolded model, only the handle fragments were fixed (see **Figure 1**). A total of 40 folded and 40 unfolded models were generated, giving 1600 possible pairs of folded-unfolded models. We have made these models available at *http://csb.stanford.edu/~adelene/hairpin_pulling_electrostatics*

Poisson-Boltzmann calculations

All Poisson-Boltzmann (PB) calculations were done with the Adaptive Poisson-Boltzmann Solver (APBS) 1.1[6]. Coarse and fine mesh grids of $272 \times 272 \times 1088$ and $160 \times 160 \times 641$ were respectively chosen, with $161 \times 161 \times 641$ grid points used (grid spacing of 1.7 and 1 respectively). The center of the hairpin structure was taken as the box center. Varying the box size, grid spacing and box center resulted in ~6% variation of ΔG_F and ΔG_U for a given $[M^+]$, but much larger variation in the absolute values of ΔG_{el}. However, trends in ΔG_F and ΔG_U with $[M^+]$

were affected in tandem, so that electrostatic trends in ΔG_{el} were consistent across different choices of parameters. Similarly, absolute values of ΔG_{el} varied significantly across the different pairs of folded and unfolded hairpin models while the trends in ΔG_{el} versus $[M^+]$ were consistent. These findings support our expectation that the specific details of the atomic models (and hence DNA-solvent dielectric boundary) do not strongly affect the electrostatic dependence of the unfolding energy on $[M^+]$[7,8].

The Mg^{2+} titration in 200 mM K^+ was slightly more sensitive to the box size due to the small calculated changes in ΔG_{el}. In this titration, a non-physical decrease in hairpin stability was observed going from 0 to 1 mM Mg^{2+} – a likely numerical artifact we were able to remove by adjusting the grid spacing to 2 Å.

For all calculations, the solvent and DNA dielectrics were set to 78.54 and 2 respectively, and the solvent-accessible probe was 1.4 Å. All ionic "radii" in APBS were set to 2 Å. However it is important to note that PB treats all ions as point charges, and the "radius" parameter only determines the distance of closest approach of the ions to the DNA. Increasing this distance to match the hydrated radius of each monovalent ion (see **Figure S5)** did not consistently improve the fit of the calculated ΔG_{el} trend to the corresponding ΔG series (data not shown).

A size-modified version of Poisson-Boltzmann theory was also used to calculate separate ΔG_{el} trends for each monovalent ion except TMA^+. The calculations were conducted using an in-house modified version of APBS[9]. In these calculations, Na^+ (with radius a), the predominant trace ion present in all measurements (see "Buffers"), was included at its final diluted concentration as the background cationic species. The titrated ionic species was then included with volume ($ak^{1/3}$), where k is a factor that scales with its parameterized volume[9].

Fitting Poisson-Boltzmann calculations to experimental data

As we could not calculate non-electrostatic contributions to ΔG with PB, we fitted calculated values of ΔG_{el} to our experimentally measured ΔG values to assess the ability of PB to capture electrostatic trends. Each calculated ΔG_{el} series, corresponding to one pair of folded and unfolded hairpin models, was fitted to the appropriate experimental series by chi-squared minimization with one free parameter (the offset on the energy scale). The averages of the fitted points are plotted in **Figures 3, 4, and S6**. For the Mg^{2+} titrations, there were minimal changes in ΔG between 5 and 10 mM Mg^{2+} for both background K^+ concentrations, and only points corresponding to these Mg^{2+} concentrations were used to perform the fitting **(Figure 4A)**. We also fit lin-log lines to each monovalent ΔG_{el} series, and the slopes (mean ± standard deviation) are reported in **Tables 1, S2 and S3**.

2. SUPPORTING FIGURES

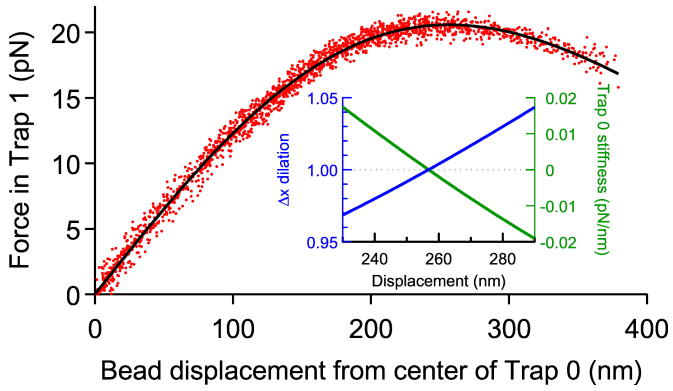

Figure S1. Calibration of the optical force clamp and correction of measured Δ*x* values. A dumbbell comprised of two beads joined by a DNA tether was trapped in 200 mM K^+ working buffer. Data (red) were obtained as the traps were separated, with the intensity of Trap 0 set to approximately half that of Trap 1. The data were well-fit by the derivative of a Gaussian function (black), and the peak of this function, corresponding to a bead displacement of approximately 258 nm from the center of Trap 0, was interpreted to be the point at which the stiffness of Trap 0 vanished. The ~50 nm region centered on this point was operationally defined as the zero stiffness region (ZSR)[10]. The derivative of the fit function (equal to local stiffness of Trap 0, *inset*), the calibrated stiffness of Trap 1 (0.24 pN/nm), and the stiffness of the DNA construct (~0.5 pN/nm, typical of hairpin force-extension curves measured in this study) were used to calculate[10] the dilation of measured Δ*x* values (*inset*) as a function of displacement. This quantity represents the measured Δ*x* normalized to the true molecular Δ*x*, and was used to rescale measured Δ*x* values to remove the displacement-dependent effect of non-zero Trap 0 stiffness. To ensure that each Δ*x* value was correctly rescaled for the Trap 1 stiffness at which the hairpin molecule was measured, the data (red) were rescaled, the fitting was repeated, and the Δ*x* dilation function was recalculated for each calibrated Trap 1 stiffness used in this study (0.24-0.29 pN/nm).

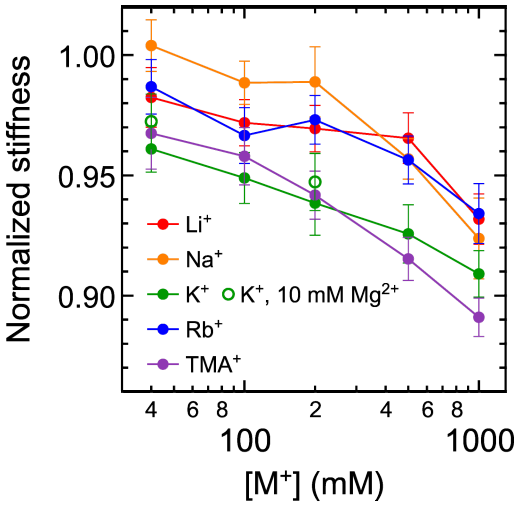

Figure S2. Relative trap stiffnesses measured by the method of Brownian fluctuations in working buffers used for data collection. The stiffnesses were normalized to that measured in water and used to rescale the absolute calibrated trap stiffnesses (and therefore measured $F_{1/2}$ values) for changes due to the refractive index, which depends on solute concentration. Points for monovalent buffers are connected to guide the eye. Stiffnesses measured for 40 or 200 mM K^+ were not significantly lower in the presence of 10 mM Mg^{2+} than in the complete absence of Mg^{2+}. Therefore stiffnesses were not measured in the remaining buffers used for the divalent titrations. Each point represents the mean of at least 10 measurements (each a separate bead) ± the standard error.

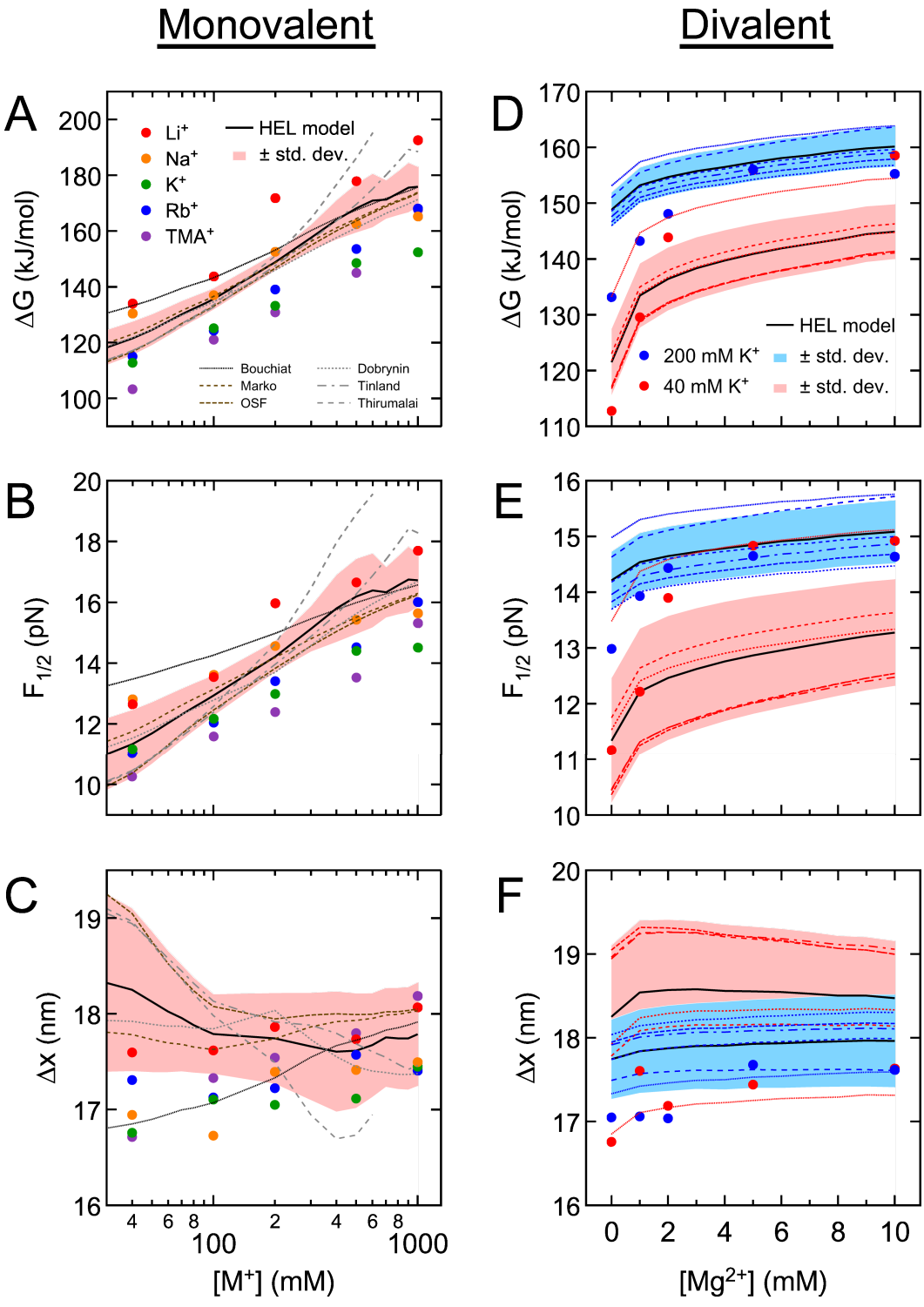

Figure S3. HEL model calculations separated by persistence length formulation.
(Caption on next page.)

The dependence of ssDNA persistence length (L_p) on ion concentration is controversial, and so we ran the HEL model using six different formulations of L_p: L_{p1}, the "bare" persistence length from Bouchiat's approximation to the WLC solution[11]; L_{p2}, the Odijk-Skolnick-Fixman electrostatically enhanced persistence length ($L_{p2} = L_{p1} + l_{OSF}$, where l_{OSF} is as defined in refs 12,13); L_{p3}, a scale-dependent persistence length suggested by Marko that is intermediate between L_{p1} and L_{p2} ($L_{p3} = L_{p1} + l_{OSF} \cdot K(q)$, where $K(q)$ is as defined in refs 14,15 and q satisfies the equation $L_{p3} \cdot q^2 = \text{force}/k_BT$)[16]; L_{p4}, as defined by Ha and Thirumalai for flexible polyelectrolytes in the large-screening limit[17]; L_{p5}, the electrostatic persistence length defined by Dobrynin[18]; and L_{p6}, an empirical, force-independent and ionic strength-dependent expression for ssDNA persistence length determined by Tinland *et al.*[19].

Here we superimpose the average predictions of ΔG **(A, D)**, $F_{1/2}$ **(B, E)**, and Δx **(C, F)** from each formulation on the plots from **Figures 3 and 4** corresponding to the monovalent **(A-C)** and divalent **(D-F)** titrations, respectively. The composite HEL predictions, in which all six formulations are used, are represented by solid black lines and shaded uncertainty envelopes as in **Figures 3 and 4**. Error bars and linear fits to the data are omitted for clarity.

L_{p1} ("Bouchiat") is the only formulation that does not include an explicit electrostatic term. L_{p2} ("OSF") and L_{p3} ("Marko") vary quadratically with the Debye screening length and are colored brown in panels A-C. L_{p4} ("Thirumalai"), L_{p5} ("Dobrynin"), and L_{p6} ("Tinland") vary linearly with the Debye screening length and are colored gray in panels A-C. The curve styles are kept consistent throughout the figure for each formulation, but in panels D-F the curves are colored to indicate $[K^+]$. The curves for L_{p4} stop at 600 mM M^+ (A-C) because the HEL model produced numerical errors using this formulation at higher $[M^+]$.

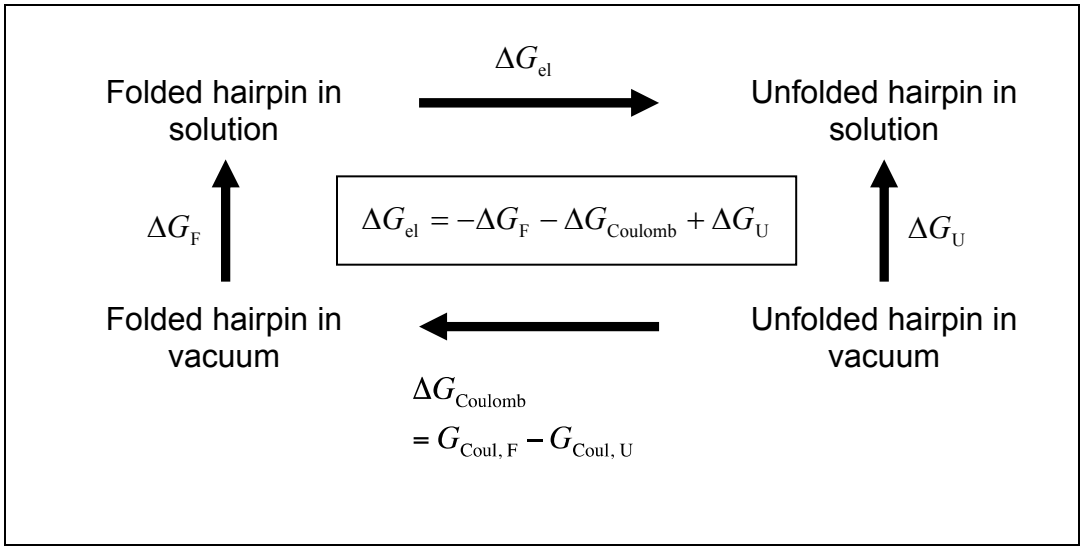

Figure S4. Thermodynamic cycle used in Poisson-Boltzmann calculations. Each calculated electrostatic hairpin unfolding energy (ΔG_{el}) included the energies of solvation of the folded (ΔG_F) and unfolded (ΔG_U) hairpin models as well as the *in vacuo* Coulombic folding energy ($\Delta G_{Coulomb}$). See **Experimental Section** for more information.

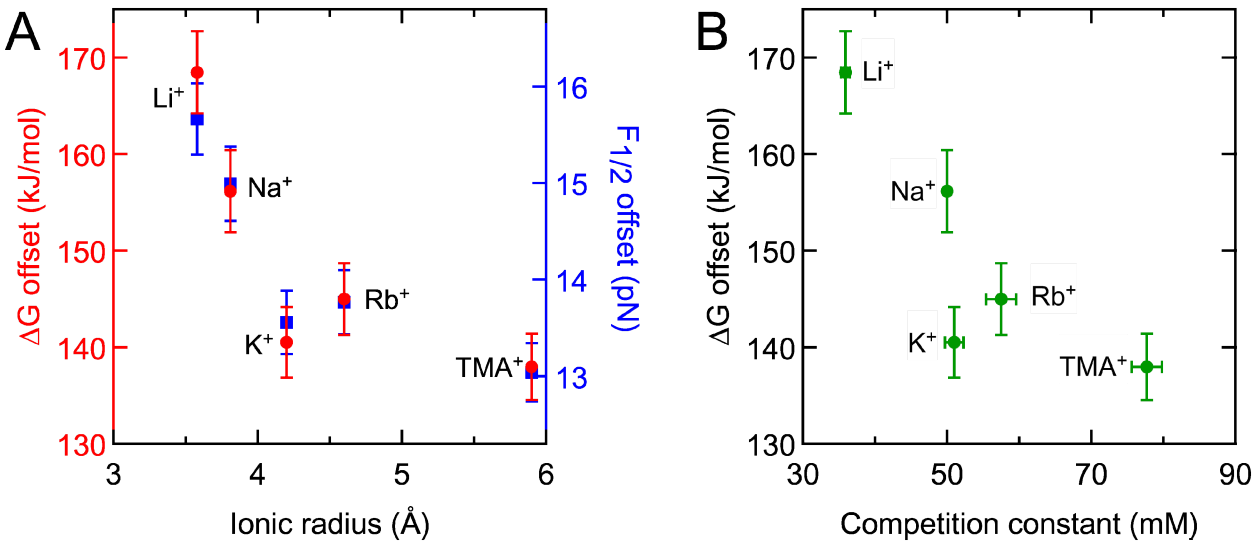

Figure S5. Correlation of measured monovalent Δ*G* values with $F_{1/2}$ values, ionic radii, and competition constants. (A) A global slope, $\mathbf{m_{global}} = 39 \pm 4$, was obtained through a linear fit (not shown) to all experimental monovalent Δ*G* data vs log[M^+] **(Figure 3A)**. This slope was used to constrain a linear fit to the Δ*G* series for each ion. The Δ*G* offset (left axis) was determined as the value of each individually fitted line at 300 mM M^+. Similarly, the $F_{1/2}$ offset (right axis) for each ion equals the value at 300 mM M^+ of a linear fit to the corresponding $F_{1/2}$ data series **(Figure 3C)**, with the slope constrained to the global value. The Δ*G* and $F_{1/2}$ offsets are thus measures of the average relative positions of the corresponding data series for each ion. Each hydrated ionic radius is the approximate distance from the ion to the oxygen atom in the first hydration shell[20,21] plus 1.4 Å for the water layer. **(B)** The same Δ*G* offsets calculated in (A) are plotted against *competition constants* for monovalent cations measured previously[22]. A competition constant characterizes the displacement of one cationic species (the background counterion, here Na^+) by another (the competing counterion, here Li^+, K^+, Rb^+ or TMA^+) from the ion atmosphere as the bulk concentration of the competing counterion is raised. The constant is defined as the concentration of the competing counterion necessary to displace half the number of background counterions that are present in the ion atmosphere in the absence of the competing counterion. The competition constants reported here were obtained from counting ions around a DNA molecule (24-bp duplex present at <1 mM) with 50 mM background Na^+ concentration. Hence, by definition, the competition constant for Na^+ is 50 mM.

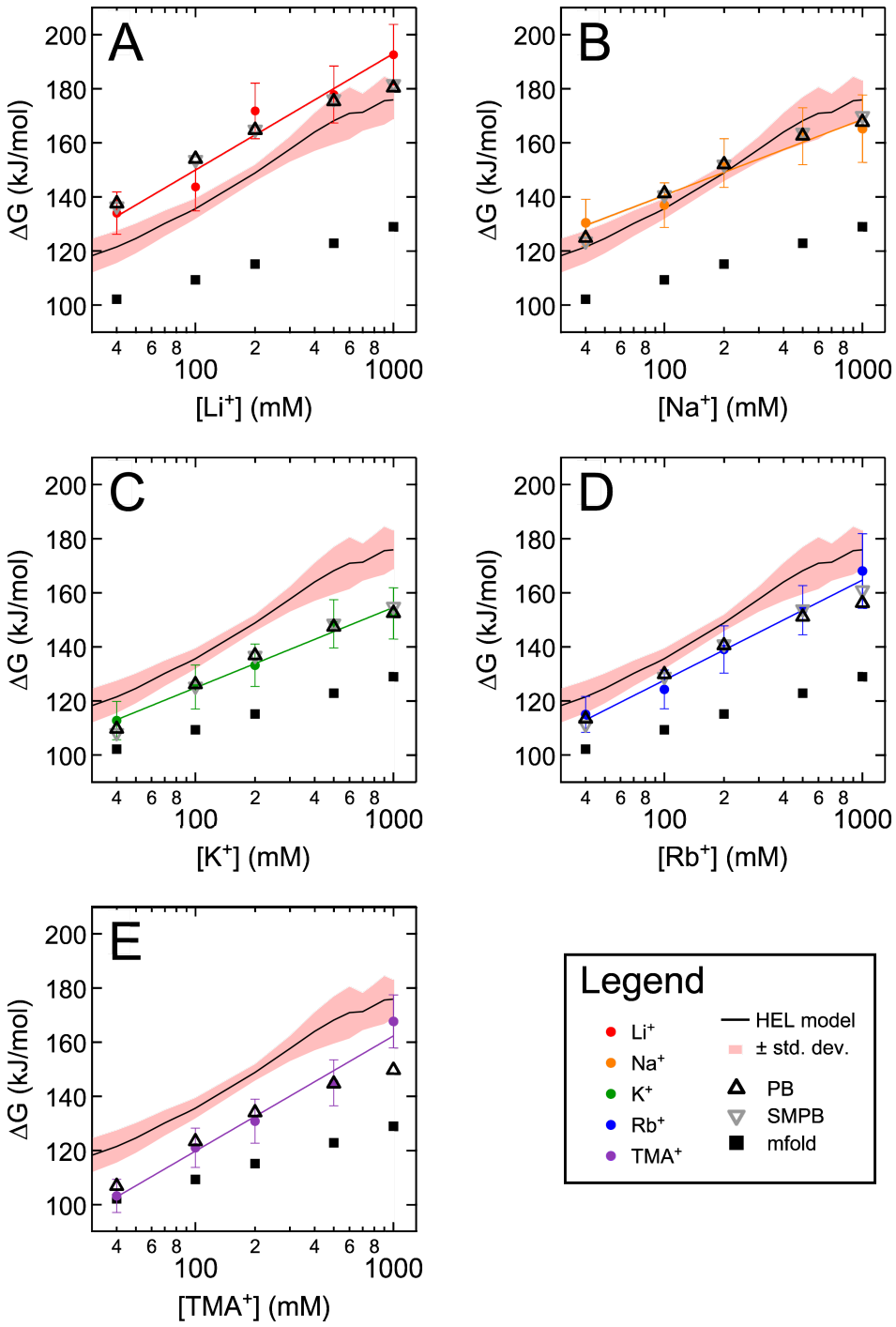

Figure S6. Gallery of Δ*G* values for monovalent titrations. Experimental Δ*G* (colored circles) are shown for Li^+ **(A)**, Na^+ **(B)**, K^+ **(C)**, Rb^+ **(D)**, and TMA^+ **(E)**. Energies from PB calculations (upward-pointing black triangles) were fit to each series by varying the overall offset in energy to minimize χ^2. Similarly fitted energies from SMPB calculations (downward-pointing gray triangles) are also shown for each ion except TMA^+. Uncertainties were smaller than the symbols for both types of calculations. Each panel also includes the energies predicted by the HEL model (black curve) and *mfold* (squares) as in **Figure 3**.

3. SUPPORTING TABLES

Table S1. Summary of HEL model predictions.

Concentration (mM)		$F_{1/2}$ (pN)	Δx (nm)	ΔG (kJ/mol)
M^+	Mg^{2+}			
40	0	11.3 ± 1.1	18.2 ± 0.9	121 ± 6
	1	12.2 ± 1.1	18.5 ± 0.9	133 ± 6
	2	12.5 ± 1.1	18.6 ± 0.8	136 ± 6
	5	12.9 ± 1.1	18.6 ± 0.8	141 ± 5
	10	13.3 ± 1.1	18.5 ± 0.7	145 ± 5
100	0	12.9 ± 0.7	17.8 ± 0.4	136 ± 4
200	0	14.2 ± 0.5	17.7 ± 0.5	149 ± 3
	1	14.5 ± 0.5	17.8 ± 0.5	153 ± 3
	2	14.6 ± 0.5	17.9 ± 0.5	155 ± 3
	5	14.8 ± 0.5	17.9 ± 0.5	157 ± 3
	10	15.1 ± 0.6	18.0 ± 0.6	160 ± 4
500	0	16.2 ± 1.2	17.6 ± 0.6	168 ± 9
1000	0	16.7 ± 0.9	17.8 ± 0.5	176 ± 7

For each combination of $[M^+]$ and $[Mg^{2+}]$, 60 calculations were conducted using different combinations of input parameters. Reported values represent the mean ± standard deviation of outputs from all successful calculations. Calculations were also done at $[M^+]$ = 30, 50, 60, 70, 80, 90, 300, 400, 600, 700, 800, and 900 mM and at $[Mg^{2+}]$ = 3, 4, 6, 7, 8 and 9 mM (with $[M^+]$ = 40 or 200 mM). All calculation results are plotted in **Figures 3 and 4**.

Table S2. Effect of varying conditions of PB calculations on the slope (m_{PB}) of ΔG_{el} versus log[M^+].

Electrostatic treatment in MD	PB force-field	Model type	m_{PB}
DC	AMBER	Standard	32.0 ± 1.2
"	"	17 nm Δx	27.8 ± 1.5 *
"	"	10 bp handles	35.6 ± 1.4 *
"	"	5 Å/bp handle rise	37.9 ± 1.2 *
"	"	No DNA handles	30.2 ± 1.4 *
GB	"	Standard	32.1 ± 1.6
LC	"	"	29.4 ± 2.8
DC	CHARMM	"	33.6 ± 1.5
GB	"	"	33.4 ± 1.7
LC	"	"	30.3 ± 2.7

The conditions used for the calculations reported in the main text are listed on the first row. "Standard" model denotes 25 bp handles with B-form geometry, and an 18-nm distance change (Δx) between the folded and unfolded states of the hairpin. Other models are the same as the "standard" model except as noted. "*" denotes conditions for which only 25 folded and 25 unfolded models were generated, instead of the standard 40. DC = constant dielectric of 80; GB = generalized Born[23], inverse Debye-Hückel length of 0.19 $Å^{-1}$; LC = low cut-off of 0.2 Å for long-range interactions in simulations (models were manually curated to ensure no steric clashes). The AMBER force-field was used for MD in all cases.

Table S3. Summary of parameters for SMPB simulations of monovalent titrations.

Ion	Ion size (Å)	m_{SMPB}	χ^2_{SMPB}
Li^+	1.00	33.7 ± 1.3	2.8
Na^+	7.16	34.6 ± 1.1	1.0
K^+	7.42	34.9 ± 1.1	0.7
Rb^+	9.47	37.2 ± 1.0	1.1
TMA^+	N.D.	N.D.	N.D.

ΔG_{el} values were calculated using the size-modified Poisson-Boltzmann algorithm[9] at the five experimental [M^+] values (40, 100, 200, 500 and 1000 mM) for Li^+, Na^+, K^+ and Rb^+. Ion sizes were parameterized according to Chu, et al.[9]; no parameterized size was available for TMA^+. A linear fit to a plot of energies versus log[M^+] for each titration (not shown) yielded the corresponding slope ($\mathbf{m_{SMPB}}$). The energies for each titration were also fitted to the corresponding experimental ΔG values using χ^2 minimization (with four degrees of freedom), with an energy offset as the only free parameter. The final χ^2 values ($\mathbf{\chi^2_{SMPB}}$) are reported.

The ΔG_{el} values obtained from SMPB fit the corresponding experimental ΔG series better in only half the cases than did the single ΔG_{el} trend from standard PB (see also **Table 1** and **Figure S6**), indicating inconsistent improvement. The ΔG_{el} slopes from SMPB increased with ionic radius, as was generally true for the experimental ΔG slopes, but the differences among slopes calculated for different ions were smaller.

Table S4. Experimental data for the Li^+ titration.

Concentration (mM)	$N_{molecules}$	$F_{1/2}$ (pN)	Δx (nm)	ΔG (kJ/mol)
40	7	12.6 ± 0.7	17.6 ± 0.4	134 ± 8
100	6	13.5 ± 0.8	17.6 ± 0.4	144 ± 9
200	8	16.0 ± 0.9	17.9 ± 0.4	172 ± 10
500	10	16.6 ± 0.9	17.7 ± 0.4	178 ± 11
1000	8	17.7 ± 1.0	18.1 ± 0.4	193 ± 11

Table S5. Experimental data for the Na^+ titration.

Concentration (mM)	$N_{molecules}$	$F_{1/2}$ (pN)	Δx (nm)	ΔG (kJ/mol)
40	7	12.8 ± 0.8	16.9 ± 0.4	130 ± 9
100	11	13.6 ± 0.8	16.7 ± 0.4	137 ± 8
200	8	14.6 ± 0.8	17.4 ± 0.4	153 ± 9
500	10	15.4 ± 0.9	17.4 ± 0.5	162 ± 11
1000	7	15.6 ± 1.1	17.5 ± 0.4	165 ± 12

Table S6. Experimental data for the K^+ titrations, in the presence and absence of Mg^{2+}.

Concentration (mM)		$N_{molecules}$	$F_{1/2}$ (pN)	Δx (nm)	ΔG (kJ/mol)
K^+	Mg^{2+}				
40	0	9	11.2 ± 0.7	16.8 ± 0.4	113 ± 7
	1	7	12.2 ± 0.7	17.6 ± 0.4	130 ± 8
	2	7	13.9 ± 0.8	17.2 ± 0.4	144 ± 8
	5	9	14.8 ± 0.8	17.4 ± 0.4	156 ± 9
	10	10	14.9 ± 0.9	17.6 ± 0.4	159 ± 10
100	0	7	12.2 ± 0.7	17.1 ± 0.4	125 ± 8
200	0	27	13.0 ± 0.7	17.0 ± 0.4	133 ± 8
	1	8	13.9 ± 0.8	17.1 ± 0.4	143 ± 8
	2	6	14.4 ± 0.8	17.0 ± 0.4	148 ± 9
	5	12	14.6 ± 0.8	17.7 ± 0.4	156 ± 9
	10	9	14.6 ± 0.8	17.6 ± 0.4	155 ± 9
500	0	7	14.4 ± 0.8	17.1 ± 0.4	148 ± 9
1000	0	12	14.5 ± 0.8	17.4 ± 0.4	152 ± 9

Table S7. Experimental data for the Rb^+ titration.

Concentration (mM)	$N_{molecules}$	$F_{1/2}$ (pN)	Δx (nm)	ΔG (kJ/mol)
40	12	11.0 ± 0.6	17.3 ± 0.4	115 ± 7
100	7	12.0 ± 0.6	17.1 ± 0.4	124 ± 7
200	9	13.4 ± 0.8	17.2 ± 0.4	139 ± 9
500	9	14.5 ± 0.8	17.6 ± 0.4	154 ± 9
1000	3	16.0 ± 1.3	17.4 ± 0.4	168 ± 14

Table S8. Experimental data for the TMA^+ titration.

Concentration (mM)	$N_{molecules}$	$F_{1/2}$ (pN)	Δx (nm)	ΔG (kJ/mol)
40	9	10.3 ± 0.6	16.7 ± 0.4	103 ± 6
100	9	11.6 ± 0.6	17.3 ± 0.4	121 ± 7
200	10	12.4 ± 0.7	17.5 ± 0.4	131 ± 8
500	8	13.5 ± 0.7	17.8 ± 0.4	145 ± 8
1000	4	15.3 ± 0.8	18.2 ± 0.4	168 ± 10

Tables S4-S8. Summaries of experimental data for titrations of Li^+ (S4), Na^+ (S5), K^+ in the presence and absence of Mg^{2+} (S6), Rb^+ (S7), and TMA^+ (S8). One value of each parameter ($F_{1/2}$, Δx and ΔG) was calculated for each molecule measured. No molecule was measured under multiple conditions. Reported values of $F_{1/2}$ and Δx represent the mean ± total propagated uncertainty, which includes the standard error on the mean (calculated by the bootstrap method) and sources of systematic uncertainty (see **Supporting Experimental Procedures**). Values of ΔG are reported similarly, but since this parameter equals the product of $F_{1/2}$ and Δx, the uncertainty in ΔG equals the uncertainties in $F_{1/2}$ and Δx added in quadrature. Relatively few molecules were measured at 1000 mM Rb^+ and TMA^+ because the high salt concentrations increased the stickiness of microscope coverslips and made it difficult to pick up dumbbells.

4. SUPPORTING REFERENCES

(1) Woodside, M. T.; Behnke-Parks, W. M.; Larizadeh, K.; Travers, K.; Herschlag, D.; Block, S. M. *Proc. Natl. Acad. Sci. U.S.A.* **2006**, *103*, 6190-5.

(2) Gal, J.; Schnell, R.; Szekeres, S.; Kalman, M. *Mol. Gen. Genet.* **1999**, *260*, 569-73.

(3) Spitzer, S.; Eckstein, F. *Nucleic Acids Res.* **1988**, *16*, 11691-704.

(4) Cornell, W. D.; Cieplak, P.; Bayly, C. I.; Gould, I. R.; Merz, K. M.; Ferguson, D. M.; Spellmeyer, D. C.; Fox, T.; Caldwell, J. W.; Kollman, P. A. *J. Am. Chem. Soc.* **1995**, *117*, 5179-97.

(5) Macke, T. J.; Case, D. A. *Molecular Modeling of Nucleic Acids* **1998**, *682*, 379-93.

(6) Baker, N. A.; Sept, D.; Joseph, S.; Holst, M. J.; McCammon, J. A. *Proc. Natl. Acad. Sci. U.S.A.* **2001**, *98*, 10037-41.

(7) Dong, F.; Vijayakumar, M.; Zhou, H. X. *Biophys. J.* **2003**, *85*, 49-60.

(8) Lipfert, J.; Chu, V. B.; Bai, Y.; Herschlag, D.; Doniach, S. *J. Appl. Cryst.* **2007**, *40*, S229-34.

(9) Chu, V. B.; Bai, Y.; Lipfert, J.; Herschlag, D.; Doniach, S. *Biophys. J.* **2007**, *93*, 3202-9.

(10) Greenleaf, W. J.; Woodside, M. T.; Abbondanzieri, E. A.; Block, S. M. *Phys. Rev. Lett.* **2005**, *95*, 208102.

(11) Bouchiat, C.; Wang, M. D.; Allemand, J.; Strick, T.; Block, S. M.; Croquette, V. *Biophys. J.* **1999**, *76*, 409-13.

(12) Odijk, T. *J. Polymer Sci. B-Polymer Phys.* **1977**, *15*, 477-83.

(13) Skolnick, J.; Fixman, M. *Macromolecules* **1977**, *10*, 944-8.

(14) Cocco, S.; Marko, J. F.; Monasson, R.; Sarkar, A.; Yan, J. *Eur. Phys. J. E Soft Matter* **2003**, *10*, 249-63.

(15) Marko, J. F.; Siggia, E. D. *Macromolecules* **1995**, *28*, 8759-70.

(16) Marko, J. F., Personal communication **2009**.

(17) Ha, B. Y.; Thirumalai, D. *Macromolecules* **1995**, *28*, 577-81.

(18) Dobrynin, A. V. *Macromolecules* **2005**, *38*, 9304-14.

(19) Tinland, B.; Pluen, A.; Sturm, J.; Weill, G. *Macromolecules* **1997**, *30*, 5763-5.

(20) Garde, S.; Hummer, G.; Paulaitis, M. E. *J. Chem. Phys.* **1998**, *108*, 1552-61.

(21) Ohtaki, H.; Radnai, T. *Chem. Rev.* **1993**, *93*, 1157-204.

(22) Bai, Y.; Greenfeld, M.; Travers, K. J.; Chu, V. B.; Lipfert, J.; Doniach, S.; Herschlag, D. *J. Am. Chem. Soc.* **2007**, *129*, 14981-8.

(23) Tsui, V.; Case, D. A. *Biopolymers* **2000**, *56*, 275-91.